Parametric Analysis of the Design Point for a Centrifugal Nuclear Thermal Rocket Fuel Element

Joel Krakower[1,2], David Austin[1], Dhruv Shah[1], and Yanni Tsetsekos[1]

[1] *Drexel University Department of Mechanical Engineering & Mechanics, 3141 Chestnut St, Philadelphia, PA 19104*
[2] *NASA Marshall Space Flight Center, MSFC, AL 35812*

joelkrakower@gmail.com

[Placeholder for Digital Object Identifier (DOI) to be added by ANS]

The Centrifugal Nuclear Thermal Rocket (CNTR) is a theoretical high-performance liquid-core nuclear thermal propulsion system. The current design under development by NASA utilizes 19 rotating Centrifugal Fuel Elements (CFEs). While the baseline parameters for the CNTR engine have been established from both systems and neutronics perspectives, a baseline for the CFEs and their mechanical design requirements has not. This paper aims to establish a mechanical baseline configuration of a CFE and quantify the effects of various design parameters in order to expand upon the existing CNTR systems model, assist future research, and inform the design and construction of a non-nuclear prototype.

I. INTRODUCTION

I.A CNTR Overview

The Centrifugal Nuclear Thermal Rocket (CNTR) is an advanced nuclear thermal propulsion (NTP) engine concept that utilizes a bubble-through liquid-fuel reactor to heat the propellant directly through multiphase heat transfer. The current design of the CNTR under development by NASA and its university partners contains 19 centrifugal fuel elements (CFEs) within a shared cylindrical moderating block. Each CFE is spun by a turbine at its top, and this rotation generates centrifugal force to retain the dense liquid uranium fuel while the lighter hydrogen propellant passes through it.

The CNTR can achieve a higher specific impulse (~1800 s) than more conventional solid-core NTP designs by operating at increased temperatures of up to 5500 K while also providing high levels of thrust.[1] This could allow for viable interplanetary transit if realized; however, much of the design of the engine has yet to be determined.

I.B CFE Overview

Currently, there are two configurations of the CFE. The first, as described in Thomas et al.,[1] is designed to have hydrogen flow radially inward from an outer hydrogen channel through a silicon carbide porous medium (PM), into a liquid uranium annulus, and then out into the center hot hydrogen core, all rotating at a controlled speed. The flow path challenges that arise from directing the hydrogen in the outer channel to power the turbine rotation are alleviated in this second configuration.

The second design, first proposed by Fisher et al.,[2] contains the same inner geometry; however, there is also a case encapsulating the porous medium which rotates with the rest of the CFE. This case divides the annulus into inner and outer channels, forcing all propellant to flow through the turbine prior to radial injection into the porous medium. A view of the entire CNTR engine with this configuration can be seen in Figure 1, while a detailed top-down view of a single CFE is shown in Figure 2.

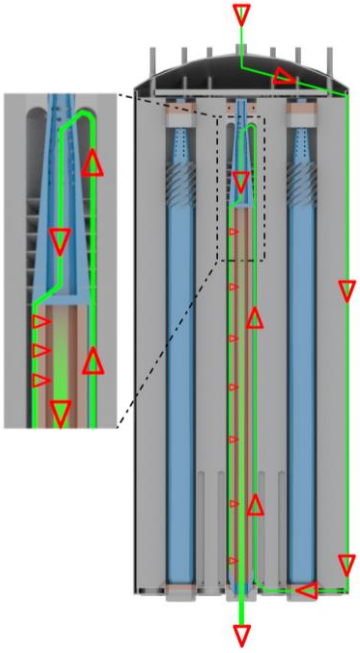

Fig. 1. Side-view schematic of the CNTR with propellant flow path and detail view of turbine portion of CFE.[2]

The CFE geometry and pitch between the CFEs play a large role in the neutronics of the engine. Recently, a study was performed showing how varying the geometry changes the neutronics,[3] however no such study exists noting how the mechanical properties of the CFE will change with its geometry. Further, there has been no direct analysis of the various mechanical effects the CFE will experience outside of heat transfer in the uranium annulus.

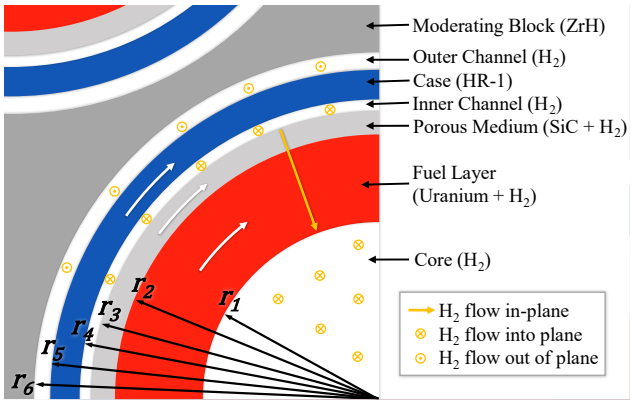

Fig. 2. Top-down cross-sectional schematic of a portion of a single CFE.

A critical function of the CFE is its ability to maintain a high rotation rate to minimize uranium fuel losses. However, given any arbitrary combination of CFE parameters—including inlet temperature, outlet pressure, CFE turbine pressure ratio, and mass flow rate—there is no guarantee that a feasible turbine capable of producing the torque required at the design point could be designed.

Before turbomachinery can be designed, this design point, consisting of the specifications required for the turbine's use case, must be determined. The most critical of these specifications is the required power output of the turbine in order to spin the CFE. The present work aims to quantify these design point specifications through modeling across a broad range of design parameters.

I.B. Nomenclature

TABLE I. Nomenclature used in this report.

Symbol	Description
A	Cross sectional area of porous SiC
a_{max}	Maximum acceleration of rocket
C_m	Torque friction coefficient for viscous flow
D_{bore}	Bearing inner bore diameter
d_{pore}	Porous medium average pore diameter
$\mathbf{F_b}$	Load vector on bearing
F_z	Axial force upon the CFE
F_0	Force relating to friction in unloaded bearings
g	Gravitational acceleration on Earth
Δh_0	Specific work done by turbine
Δh_{ss}	Isentropic enthalpy drop
k_1	Darcian permeability coefficient
k_2	Non-Darcian permeability coefficient
l	Length of the CFE
$\dot{m}$	Mass flow rate of propellant through CFE
m_{CFE}	Mass of the CFE
M_{bear}	Frictional torque of a single bearing
M_{visc}	Viscous torque
$M_{TCF,lam}$	Torque in laminar Taylor-Couette flow
Nu_ω	Rotational Nusselt number
N_s	Turbine specific speed
P_1	Turbine outlet pressure
P_2	Pressure at porous medium inner wall
P_3	CFE core pressure
ΔP_{cent}	Centripetal pressure of uranium layer
Q	Volumetric flow rate of propellant
r_1	Inner radius of uranium layer
r_2	Inner radius of porous medium
r_3	Outer radius of porous medium
r_4	Inner radius of case
r_5	Inner radius of outer channel
r_6	Outer radius of outer channel
r_{turb}	Radius of the turbine inlet
Re_z	Axial Reynolds number
Re_ω	Rotational Reynolds number
T_1	Turbine outlet temperature
T_2	Porous media inner wall temperature
T_3	Core temperature
TWR	Thrust-to-weight ratio
u_z	Axial propellant velocity
v_s	Darcian velocity
$\dot{W}$	Turbine work rate
ε	Apparent porosity of porous medium
η_{ts}	Turbine total-to-static efficiency
μ	Dynamic viscosity of propellant
μ_f	Bearing friction coefficient
ν	Kinematic viscosity of propellant
ν_s	Isentropic velocity ratio
ρ_H	Hydrogen propellant density
$\rho_U(r)$	Uranium-hydrogen mixture density profile
ω	CFE rotation rate

II. METHODOLOGY

Baseline geometry of the CFE was adapted from parameters previously used by Keese[4] and referred to by prior authors as "Design 1". This configuration was modified to include the addition of an outer case to match the propellant flow path proposed by Fisher et al.[2] The relevant design parameters for this configuration can be found in Table II and Table III.

Using these parameters as inputs, design point requirements and properties of the CFE were calculated to characterize performance of the system.

To quantify the effects of design modifications on the system, the eight parameters in Table II were swept across a range of possible values. The system was characterized at 50 possible values of each parameter. Each parameter was varied individually, while all other parameters were held constant. Table III contains parameters which were held constant across all configurations in this study.

TABLE II. Parameters studied in sweep of system.

Parameter	Baseline Value	Sweep Range	Relative Range
P_3	10 MPa	5 MPa – 20 MPa	0.5 – 2
T_1	450 K	225 K – 900 K	0.5 – 2
$\dot{m}$	.108 kg/s	0.054 kg/s – 0.216 kg/s	0.5 – 2
r_5	56 mm	55 mm – 84 mm	0.982 – 1.5
$(r_6 - r_5)$	3 mm	1.5 mm – 6 mm	0.5 – 2
ω	7000 rpm	3500 rpm – 14,000 rpm	0.5 – 2
ν_s	0.6961	0.3481 – 0.7448	0.5 – 1.07
l	0.84 m	0.42 m – 1.68 m	0.5 – 2

TABLE III. Fixed parameters in the system.

Parameter	Value
Uranium inner radius r_1	30 mm
PM inner radius r_2	45 mm
PM outer radius r_3	49 mm
Case thickness $(r_5 - r_4)$	5 mm
PM wall temperature T_2	1494 K
CNTR thrust-to-weight ratio TWR	1.3
Baseline bearing friction load F_0	450 N
Bearing friction coefficient μ_f	0.0015
PM apparent porosity ε	0.36

II.A. Determination of Turbine Outlet Pressure

The pressure at the PM inner wall is considerably higher than the core pressure due to the centripetal force of the uranium fuel. The inner wall pressure can be expressed as the sum of the core and centripetal pressures, shown in Eq. (1).

$$P_2 = P_3 + \Delta P_{cent} \tag{1}$$

This centripetal pressure depends upon the density profile within the uranium fuel layer. A one-dimensional finite difference model of heat transfer in the system was adapted from prior work by Keese[4] to determine the distributions of voids, density, and pressure within the uranium fuel layer. For each set of parameters, a 400-cell model was created, assuming a wall temperature of 1494 K. The total additional pressure due to centripetal forces was calculated through numerical integration of Eq. (2).

$$\Delta P_{cent} = \omega^2 \int_{r_1}^{r_2} r \rho_U(r) dr \tag{2}$$

In this model and later calculations, hydrogen property data for temperatures below 1000 K was compiled from Refprop software[5] released by NIST. For higher temperatures, NASA's Chemical Equilibrium with Applications software[6] was used to ensure that the effects of dissociation were fully taken into account.

It is important to note that this model used a fixed heating profile based upon the neutronics model generated by Walters[3] for a particular geometry, and does not account for changes to the neutronics of the system with each parameter.

A much smaller pressure gradient will also exist pointing radially inwards across the PM. The pressure drop through the PM is determined using the Darcy-Forchheimer equation, as seen in Eq. (3), for compressible flow through porous media:

$$\frac{P_1^2 - P_2^2}{2P_2(r_3 - r_2)} = \frac{\mu v_s}{k_1} + \frac{\rho_H v_s^2}{k_2} \tag{3}$$

where the Darcian velocity, v_s, is the volumetric air flow rate over the cross-sectional area normal to the flow as defined in Eq. (4).

$$v_s = \frac{\dot{m}}{\rho A} \tag{4}$$

As no experimental permeability data exists for hydrogen flow through porous silicon carbide, an approximation using air flow is considered for subsequent calculations.[7] A correlation between the apparent porosity, ε, and the resulting average pore size in experimental samples of SiC is defined in Eq. (5). The correlation is subsequently used in an empirical relationship between pore diameter and the resulting Darcian permeability, k_1, as seen in Eq. (6).

$$d_{pore} = 0.41968 e^{0.06579\epsilon} \tag{5}$$

$$k_1 = \frac{2.25}{150} \epsilon d_{pore}^2 \tag{6}$$

The Darcian and non-Darcian permeability coefficients, k_1 and k_2 respectively, are fit to the Darcy-Forchheimer equation to yield the correlation defined in Eq. (7) (Ref. 7).

$$k_2 = \exp\left(-\frac{1.71588}{k_1^{0.08093}}\right) \tag{7}$$

Using the properties of the hydrogen through the PM and the correlation for the permeability coefficients, the inlet pressure to the PM can be calculated using Eq. (8).

$$P_1 = \sqrt{P_2^2 + 2P_2\left(\frac{\mu v_s}{k_1} + \frac{\rho_H v_s^2}{k_2}\right)(r_3 - r_2)} \tag{8}$$

Negligible pressure losses were assumed through the inner channel around the PM, making this pressure equivalent to the turbine outlet pressure.

II.B. Determination of Power Losses

Power requirements for the turbine were analyzed for steady-state operation. To maintain consistent rotation, the turbine must offset the expected moment due to viscous flow around the fuel element and friction from each bearing. This work rate was calculated using Eq. (9).

$$\dot{W} = \omega M_{visc} + \omega \sum_{i=1}^{n} M_{bear_i} \tag{9}$$

II.B.1. Viscous Losses

The flow through the channel around the CFE can be most accurately described as Taylor-Couette-Poiseuille flow, or TCPF, consisting of axial flow between two concentric cylinders when one or both cylinders are

rotating.[8] Rotational and axial Reynolds numbers are defined in Eq. (10) and Eq. (11), respectively, each with regards to the radial clearance.

$$Re_\omega = \frac{\omega r_5 (r_6 - r_5)}{\nu} \quad (10)\ (\text{Ref. } 8)$$

$$Re_z = \frac{v_z (r_6 - r_5)}{\nu} = \frac{\dot{m}}{\mu \pi (r_6 + r_5)} \quad (11)\ (\text{Ref. } 8)$$

The case of no axial flow is known simply as Taylor-Couette flow. For laminar Taylor-Couette flow, the moment due to an inner cylinder rotating can be calculated using Eq. (12) below.

$$M_{TCF,lam} = \frac{4\pi\mu l\omega}{r_5^{-2} - r_6^{-2}} \quad (12)\ (\text{Ref. } 9)$$

For regimes with turbulent or axial flow, a rotational Nusselt number which describes the ratio of the observed torque to actual torque can be defined. This Nusselt number is generally thought to be a function of three parameters, namely each Reynolds number and the ratio of the inner and outer radii,[8,10] as in Eq. (13).

$$Nu_\omega = \frac{M_{visc}}{M_{TCF,lam}} = f\left(Re_\omega, Re_z, \frac{r_5}{r_6}\right) \quad (13)$$

Alternatively, some authors use a torque coefficient,[8] which can be converted to the Nusselt number using Eq. (14).

$$C_m \equiv \frac{M_{visc}}{2\rho_H l \pi r_5^4 \omega^2} = \frac{2}{Re_\omega \left(1 + \frac{r_5}{r_6}\right)\left(\frac{r_5}{r_6}\right)} Nu_\omega \quad (14)$$

The existing literature reviewed lacks experimental or computational torque data at the design conditions of the CFE. However, Taylor-Couette flow without any axial component has been well-researched, and several correlations exist for rotational Reynolds numbers on the order of the CFE.[9,10,11]

The empirical formula in Eq. (15) was adapted from Lewis and Swinney[10] to calculate an approximate Nusselt number for the case of no axial flow, where variation due to the radius ratio is considered negligible.

$$\log_{10}\left[Nu_\omega(Re_\omega)|_{Re_z=0}\right] \approx -.006360\,(\log_{10} Re_\omega)^3 + .13490\,(\log_{10} Re_\omega)^2 - .1150 \log_{10}(Re_\omega) - 0.232091 \quad \text{for } 13{,}000 \le Re_\omega \le 10^6 \quad (15)$$

Some TCPF research includes torque coefficients for axial Reynolds numbers much closer to that within the CFE and for similar radius ratios, but at lower rotational Reynolds numbers. Extrapolating the trends reported by Yamada[8] suggests that axial flow through the outer channel is likely to slightly increase the viscous torque. For calculation purposes, this increase was estimated as 10%, as shown in Eq. (16).

$$Nu_\omega\left(Re_\omega, Re_z, \frac{r_5}{r_6}\right) \approx 1.1\, Nu_\omega(Re_\omega)|_{Re_z=0} \quad (16)$$

The torque was then calculated from the Nusselt number and the laminar torque using Eq. (17).

$$M_{visc} \approx \left[1.1\, Nu_\omega(Re_\omega)|_{Re_z=0}\right] \frac{4\pi\mu l\omega}{r_5^{-2} - r_6^{-2}} \quad (17)$$

II.B.2. Bearing Losses

The frictional moment due to the bearings is the sum of friction across each bearing in the CFE. The analyzed design included three journal ball bearings due to their minimal lubrication requirements. Eq. (18) can be used to approximate frictional moment in rolling-element bearings.

$$M_{bear} = \mu_f \|\boldsymbol{F_b}\| \frac{D_{bore}}{2} \quad (18)$$

However, some experimental work has shown that this frictional moment does not approach zero at very low loads, and some baseline level of friction remains.[12,13] Eq. (19) contains a modification of Eq. (18) used to account for this baseline friction.

$$M_{bear} = \mu_f (\|\boldsymbol{F_b}\| + F_0) \frac{D_{bore}}{2} \quad (19)$$

The expected static loads on the bearings in this system are purely axial and due to the inertia of the CFE as the rocket accelerates. To allow for thermal expansion, the bottom two bearings were considered to have free movement axially within the CNTR, leading to the loading configuration in Table IV.

TABLE IV. Bearing configuration parameters.

Bearing #	Location	D_{bore}	$\|\mathbf{F_b}\|/F_z$
1	Top	20 mm	100%
2	Middle	20 mm	0%
3	Bottom	60 mm	0%

The axial force upon this top bearing is simply the force needed to accelerate the CFE and is given by Eq. (20).

$$F_z = -m_{CFE} a_{max} \quad (20)$$

The maximum rocket acceleration was calculated using Eq. (21), using the thrust-to-weight ratio of the unloaded engine,[14] assuming the use of a ZrH moderator.

$$a_{max} = (TWR)(g) \quad (21)$$

The mass of the CFE was estimated as the sum of the mass of the porous medium, case, and uranium. The uranium mass was determined using the previously calculated density profile. The mass of other components was considered to be negligible.

II.C. Turbine Selection

II.C.1 Design Point

Now that the design requirements of the turbine have been determined, the most appropriate type of turbine can be chosen. Turbine selection is a process that requires careful consideration of the design requirements, dimensionless characteristic parameters, and the turbine's specific use case. The design requirements indicate that the turbine will only need to produce enough power to overcome viscous losses from the hydrogen and friction

losses from the bearing. It will operate with a low mass flow rate, a low pressure ratio to maintain optimal turbopump operating parameters, and a high outlet pressure, *O(~10 MPa)*, to aid the heat transfer in the uranium annulus.

II.C.2 Specific Speed

The most critical dimensionless parameter for turbine selection is the specific speed, N_s. The specific speed of the turbine is calculated using Eq. (22) below.

$$N_s = \frac{\omega\sqrt{Q}}{\Delta h_{ss}^{3/4}} \tag{22}$$

Where:

$$\Delta h_{ss} = \frac{\Delta h_0}{\eta_{ts}} \tag{23}$$

The total-to-total enthalpy drop can be expressed with Eq. (24).

$$\Delta h_0 = \frac{\dot{W}}{\dot{m}} \tag{24}$$

The specific speed influences turbine selection as seen in the Cordier Diagram in Figure 3. The lowest specific speeds use drag turbines, while medium range specific speeds are ideal for radial turbines. Axial turbines generally can operate at any given specific speed but will have varying efficiencies depending on other dimensionless characteristics like flow coefficient and loading coefficient.

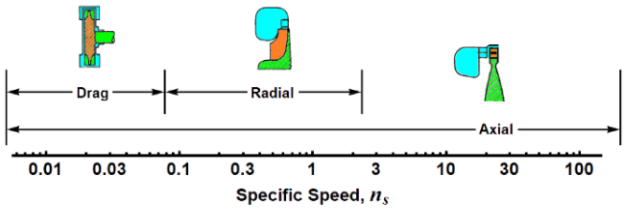

Fig. 3. Turbine specific speed ranges.[15]

II.C.3 Turbine Use Case

The most difficult aspect of turbine selection to quantify is the turbine use case, as it is mostly subjective. It is important to note that multiple types of turbines can achieve the same power production with high efficiencies in ideal circumstances. To properly select a turbine for a given use case, the flow conditions at the turbine inlet and outlet must be considered. The inlet flow conditions will be a form of turbulent TCPF, possessing both tangential and axial components. The CFE flow path in the configuration which includes a case will require a flow turning of 180° between where the hydrogen exits the outer channel and enters the porous media inlet channel. The flow resistance of a 180° annular bend heavily depends on the size of the inlet into the inner channel from the outer annulus.[16] Having an inlet to the inner hydrogen channel of a large enough size to prevent significant resistance would prove to be a design challenge as the CFE will require a shaft to rotate and the flow path from the outer hydrogen channel to the inner hydrogen will be blocked. As such, perforations in the shaft or another mechanism connecting the two channels will be required. The flow will also need to be guided up to the radius of the inner hydrogen channel resulting in either acceleration or diffusion depending on the ratio between the channel annulus area and the turbine outlet area.

II.C.4 Preliminary Selection

The design considerations and flow conditions of the CFE point to a radial turbine as a preliminary choice before considering the specific speed. Radial turbines are more compact and can keep engine mass low. Additionally, they can deliver a larger specific power than an equivalent axial stage,[17] which allows the use of fewer stages. The flow conditions, specifically the required flow turning for this configuration and the significant inlet tangential velocity also point towards a radial turbine. Radial turbines extract work from a rotating fluid by turning it 90° from a radial inlet to an axial outlet. Across the blade, the tangential velocity in the stationary frame is reduced to zero, so a higher tangential velocity will produce more work.

III. RESULTS

The CFE design point calculated for the baseline configuration can be found in Table V. For this configuration, the specific speed confirms that a radial turbine would be the most effective choice for the rotation of the CFE. The design point will vary based on changes in the input parameters in Table II. It is again important to note that these results are not coupled with any neutronic codes.

TABLE V. Calculated baseline configuration properties.

Property	Value
Turbine outlet pressure P_1	13.754 MPa
Porous medium wall pressure P_2	13.750 MPa
CFE mass m_{CFE}	51.70 kg
Turbine work rate $\dot{W}$	153.5 W
Bearing power losses	*32.0 W*
Viscous power losses	*121.6 W*
Turbine inlet radius r_{turb}	5.35 cm
Turbine efficiency η_{ts}	0.896
Turbine specific speed N_s	0.362

The turbine outlet pressure is shown in Figure 4 across the examined input parameter ranges. Only those parameters which affect the turbine outlet pressure are shown. The turbine outlet pressure will affect the turbine inlet pressure based on the pressure ratio. Higher outlet pressures for the same pressure ratio will result in higher inlet pressures and will change the inlet and outlet flow conditions accordingly. The core pressure and the rotation rate have the strongest influence on turbine outlet pressure.

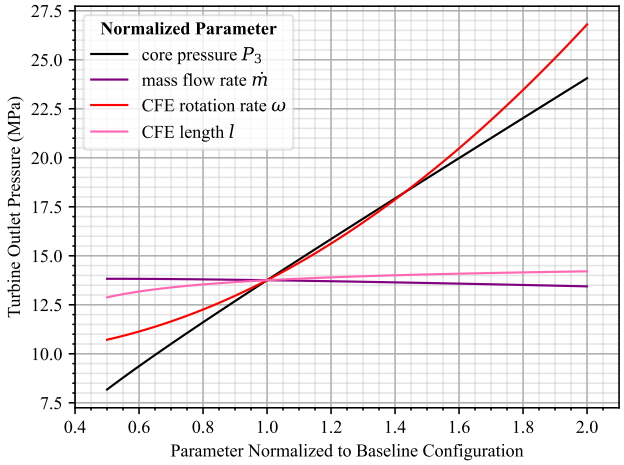

Fig. 4. Variation of turbine outlet pressure as a function of swept parameters.

The variation of the CFE mass with relevant input parameters is shown in Figure 5. Engine mass is a critical parameter for spaceflight, as it directly influences the necessary delta-V.

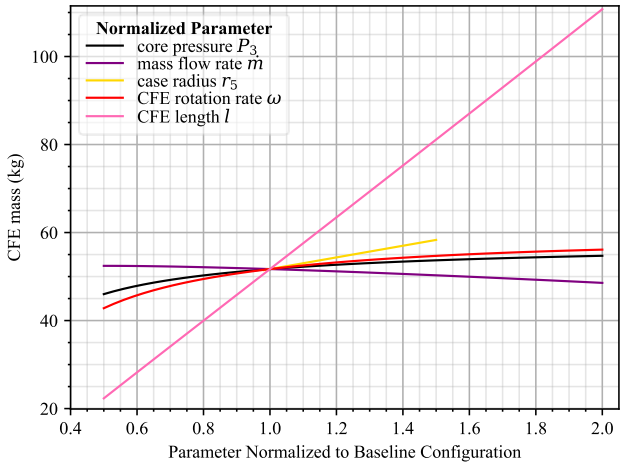

Fig. 5. Variation of CFE mass as a function of swept parameters.

The total turbine power and individual components due to viscous and bearing losses are shown across the examined parameter range in Figures 6, 7, and 8, respectively. Turbine power is the most critical parameter for the turbine design as it determines the turbine inlet radius and generally, the size of the overall turbine. The CFE rotation rate and the case radius are the two most influential parameters for both the viscous and friction losses.

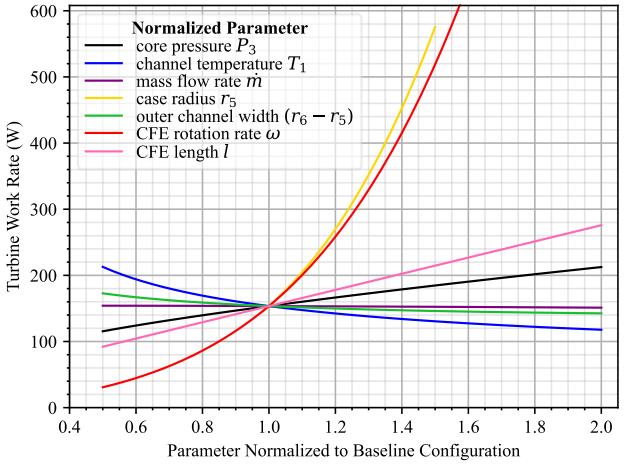

Fig. 6. Variation of total turbine power requirements as a function of swept parameters.

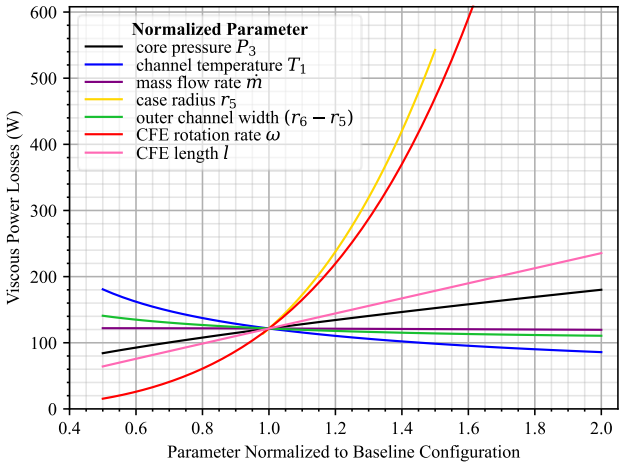

Fig. 7. Variation of power requirements due to viscous losses as a function of swept parameters.

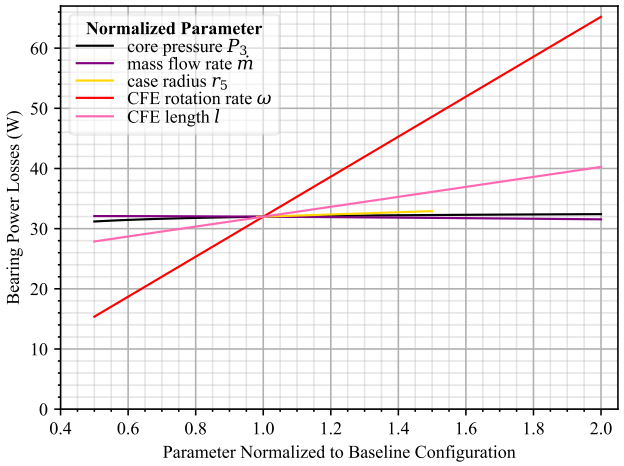

Fig. 8. Variation of power requirements due to bearing losses as a function of swept parameters.

The turbine inlet radius, efficiency, and specific speed are shown in Figures 9, 10, and 11, respectively. The efficiency shows noticeable discontinuities when certain parameters are varied, which correspond to changes in the number of turbine blades.

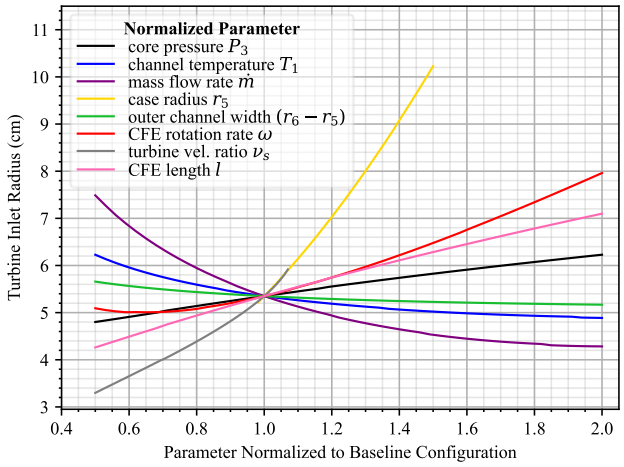

Fig. 9. Variation of turbine inlet radius as a function of swept parameters.

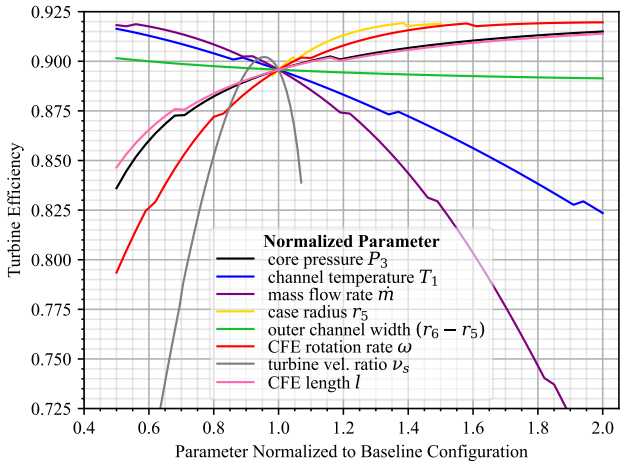

Fig. 10. Variation of turbine efficiency as a function of swept parameters.

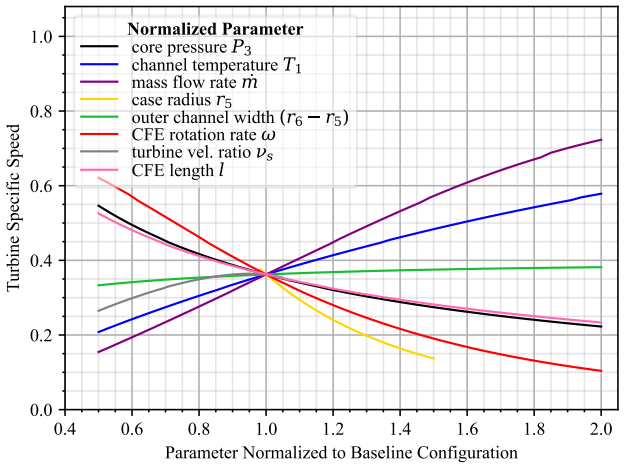

Fig. 11. Variation of turbine specific speed as a function of swept parameters.

IV. CONCLUSIONS

An ideal CFE design from a mechanical perspective would include the smallest and lightest possible turbine which is able to achieve the desired rotation rate.

The calculated operational parameters of the turbine fall well within the acceptable range for a radial turbine. However, one of the limiting factors upon the CNTR geometry appears to be the radius of the turbine, which approaches the outer radius of the CFE. Reducing the diameter of the case appears to be the most effective method to reduce this turbine radius, as shown in Figure 9.

The isentropic velocity ratio appears, at first glance, to be an ideal candidate for manipulation in order to increase the turbine efficiency, however these efficiency values are based on loss correlations.[18] The incidence loss due to the relative flow inlet angle for the design point is generally assumed to be negligible, and this analysis did not take incidence losses into account. However, at low velocity ratios it is expected that these losses will become dominant, and velocity ratios below the baseline value are not recommended.

Due to both the radial size of the turbine and the utilization of a rotating case layer which is not present is some designs, it is likely that the pitch between CFEs may need to be increased when using this CFE design. Both of these factors can be minimized by keeping the case as thin as possible, which would have the additional benefits of reducing weight and the impact on neutronics of the system.

A focus of future work will be to integrate this mechanical systems model of the CFE with a neutronics model of the engine, based on prior work by Walters.[3] The authors are also in the process of developing a non-nuclear CFE prototype which will build upon this work and be used to test the mechanical performance of the CFE.

ACKNOWLEDGMENTS

This work was supported by the Space Technology Mission Directorate (STMD) of the National Aeronautics and Space Administration through the Space Nuclear Propulsion (SNP) project.

The authors would like to give special thanks to Calix Ceramics for expertise in manufacturing, as well as Michael Houts, Thomas Godfroy, Mitchell Schroll, Omar Mireles, and Derek O'Neal from NASA MSFC for their programmatic and technical help.

REFERENCES

1. D. THOMAS et al., "Establishing the Feasibility of the Centrifugal Nuclear Thermal Rocket," *AIAA Propulsion and Energy Forum*, virtual event, American Institute of Aeronautics and Astronautics, August 02-11 2021.
2. E. FISHER et al., "CNTR: Explanation of Propellant Flow and Description of Initial Experiments," *2020 ANS Virtual Winter Meeting*, virtual event, American Nuclear Society, 2020.
3. W. J. WALTERS, "Neutronic Evaluation and Optimization of the Centrifugal Nuclear Thermal Rocket Concept." *CNTR Internal* (2022).
4. J. KEESE, *Thermal Model of a Centrifugal Nuclear Thermal Propulsion System*, The University of Alabama in Huntsville, Huntsville, Alabama (2022).
5. Reference Fluid Thermodynamic and Transport Properties Database Version 10, National Institute of Standards and Technology.
6. Chemical Equilibrium with Applications, National Aeronautics and Space Administration.
7. A. DEY et al., "Permeability and Nanoparticle Filtration Assessment of Cordierite-Bonded Porous SiC Ceramics," *In Industrial & Engineering Chemistry Research*, **52**, 51 (2013). DOI: 10.1021/ie402876v
8. Y. YAMADA, "Torque Resistance of a Flow between Rotating Co-Axial Cylinders Having Axial Flow," *Bulletin of JSME*, **5**, 20 (1962). DOI: 10.1299/jsme1958.5.634
9. D. P. M. VAN GILS et al., "Torque Scaling in Turbulent Taylor-Couette Flow with Co- and Counterrotating Cylinders," *Physical Review Letters*, **06**, 2 (2011). DOI: 10.1103/PhysRevLett.106.024502
10. G. S. LEWIS and H. L. SWINNEY, "Velocity Structure Functions, Scaling, and Transitions in High-Reynolds-Number Couette-Taylor Flow" *Physical Review E*, **59**, 5 (1999). DOI: 10.1103/physreve.59.5457
11. GROSSMAN et al., "High-Reynolds Number Taylor-Couette Turbulence," *Annual Review of Fluid Mechanics*, **48**, 1 (2016). DOI: 10.1146/annurev-fluid-122414-034353
12. Y. WANG et al., "Investigation on frictional characteristic of deep-groove ball bearings subjected to radial loads," *Advances in Mechanical Engineering*, **7**, 7 (2015). DOI: 10.1177/1687814015586111
13. K. E. VIDYASAGAR et al., "An exploration of frictional and vibrational behaviors of textured deep groove ball bearing in the vicinity of requisite minimum load," *Friction*, **9**, 6 (2021). DOI: 10.1007/s40544-021-0495-3
14. M. SCHROLL, "Performance Analysis of a Centrifugal Nuclear Thermal Rocket Engine," *HP-NTP Workshop*, Huntsville, Alabama, The University of Alabama in Huntsville, November 04 2022.
15. D. NIKITAEV et al., "Nuclear Thermal Propulsion Turbomachinery Modeling," *Nuclear and Emerging Technologies for Space 2022*, Cleveland, OH, May 8-12 2022, American Nuclear Society. DOI: 10.13182/NETS22-38690
16. I. E. IDEL'CHIK, *Handbook of Hydraulic Resistance*, D. GRUNAER, Ed., Israel Program for Scientific Translations, Jerusalem, Israel (1966).
17. N. C. BAINES, *Axial and Radial Turbines*, Concepts ETI, White River Junction, Vermont (2003).
18. J. T. KRAKOWER, "Design and Performance Analysis of a Radial-Inflow Turbine for the Centrifugal Nuclear Thermal Rocket," *CNTR Internal* (2023).